ELSEVIER

Surface Science 472 (2001) 125–132

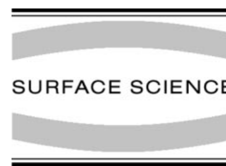

www.elsevier.nl/locate/susc

Determining adsorbate structures from substrate emission X-ray photoelectron diffraction

Matthias Muntwiler [a,b,*], Willi Auwärter [a], Felix Baumberger [a], Moritz Hoesch [a,b], Thomas Greber [a], Jürg Osterwalder [a]

[a] *Physik-Institut, Universität Zürich, Winterthurerstrasse 190, CH-8057 Zürich, Switzerland*
[b] *SLS Project, Paul Scherrer Institut, CH-5232 Villigen PSI, Switzerland*

Received 6 August 2000; accepted for publication 13 October 2000

Abstract

A new substrate emission X-ray photoelectron diffraction method that subtracts a clean substrate measurement from a measurement of the adsorbate-covered sample is able to reveal important adsorbate–substrate registry information while it suppresses disturbing substrate effects in the diffractograms. Short measurement times and an unambiguous data quality allow for a quick and convincing structural characterization of homogeneous adsorbate layers. The data processing and analysis methods are illustrated with experimental h-BN/Ni(1 1 1) data and multiple-scattering calculations. © 2001 Elsevier Science B.V. All rights reserved.

Keywords: Electron–solid diffraction; photoelectron diffraction; Surface structure, morphology, roughness, and topography; Boron nitride; Nickel

1. Introduction

Over the last years, X-ray photoelectron diffraction (XPD) has developed into a more and more quantitative tool for obtaining surface structure data, reaching in some cases the accuracy of quantitative low-energy electron diffraction (LEED). For specific geometries, XPD yields even superior results in terms of ambiguity because certain structural parameters can be extracted directly from the experimental data, while LEED always has to rely on sophisticated theoretical simulation of $I(V)$ curves for a series of trial structures and the associated R-factor analysis. Due to the dominant forward-scattering signals in XPD, stereographically projected gray-scale pictures of experimental and theoretical angular distributions of core-level photoemission allow for an intuitive visual comparison, and in various cases nearest-neighbour directions can immediately be read out [1,2]. For measuring the internal geometries of adsorbate layers or ultrathin epitaxial films, this approach has been vastly successful using photoemission signals from within the overlayers.

However, such experiments usually do not give any information on the overlayer–substrate registry, i.e. the adsorbate bonding site in the surface

* Corresponding author. Address: Physik-Institut, Universität Zürich, Winterthurerstrasse 190, CH-8057 Zürich, Switzerland. Tel.: +41-1-635-6697; fax: +41-1-635-5704.
E-mail address: m.muntwiler@physik.unizh.ch (M. Muntwiler).

0039-6028/01/$ - see front matter © 2001 Elsevier Science B.V. All rights reserved.
PII: S0039-6028(00)00928-6

unit mesh. Forward-scattering signals of the adsorbate emission containing this information are directed into the crystal and cannot be measured. Only in rare cases the much weaker backscattering signals of the type adsorbate emission – substrate scattering have been observed [3]. Unfortunately,these features depend strongly on high backscattering cross-sections and low thermal vibrations – constraints which are hardly fulfilled if light elements are involved.

The substrate emission perspective, if the adsorbate structure was projected into the vacuum only by electrons originating from atoms in the top substrate layer, would provide reliable structural information. This has been demonstrated in a recent study of Gd films on W(1 1 0) [4,5]. In this system, the photoemission signal from the tungsten atoms right at the interface can be separated from the contribution of deeper layers due to their interface core-level shift. But again, this case represents a particularly favourable situation with a large shift, and this technique is not generally applicable.

In this article, we attend to the question whether the same information can be recovered from the full substrate emission signal. The drawback here is that real diffractograms are dominated by scattering inside the substrate because electrons originating from several substrate layers are observed. If, additionally, the scattering cross-sections of the substrate atoms are higher than the ones of the adsorbate atoms, the substrate dominance gets even stronger. It will be shown that this dominance of substrate scattering can be significantly reduced by subtracting a measurement of the clean substrate sample from the measurement of the adsorbate-covered sample. The same procedure applied to corresponding model calculations leads to experimental and theoretical difference data sets that can be successfully compared to each other. It is even possible to identify spots in the experimental difference data as forward-focusing directions between top layer substrate and adsorbate atoms.

As an example, measurements and simulations of a monolayer hexagonal boron nitride film (h-BN) on top of a nickel (1 1 1) surface will be discussed. This system has already been examined in a LEED study [6] and an adsorbate emission XPD study [7]. The latter one finds only the internal film structure and its orientation but no evidence of its lateral registry relative to the substrate. LEED patterns give a 1×1 symmetry and scanning tunneling microscopy (STM) images show atomic corrugations with the periodicity of the substrate lattice. Symmetry considerations suggest three possible interface geometries which we label according to the nitrogen bonding site as ‘on top’, ‘hcp’ and ‘fcc’ (see Fig. 1). The LEED study favours the N-top geometry based on an *R*-factor comparison of experimental and simulated *I–V* curves. This result is finally confirmed by the XPD data presented here.

2. Experimental

The measurements have been done in a modified Vacuum Generators ESCALAB 220 [8]. By means of a computer-controlled two-axis manip-

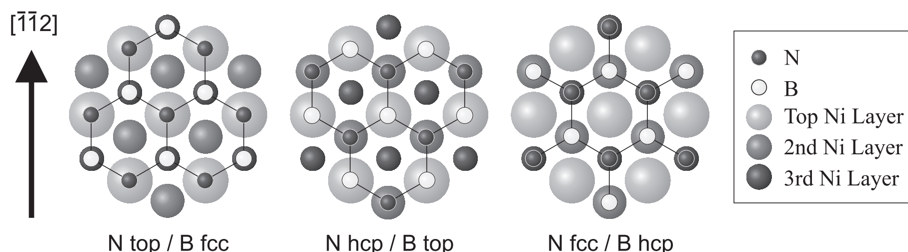

Fig. 1. Top view of the only three h-BN/Ni(1 1 1) high-symmetry structure models that remain possible after defining the orientation of the h-BN sheet with respect to the Ni(1 1 1) surface. They are distinguished by the nitrogen adsorption site. The [$\bar{1}\,\bar{1}\,2$] direction of the Ni crystal lies in the (1 1 1) surface plane. The lattice parameter of the Ni(1 1 1) surface is 2.49 Å.

ulator and an electron energy analyser with the angular resolution set to about 5° angle-resolved photoelectron intensity patterns over the full hemisphere above the sample are conveniently recorded.

The h-BN/Ni(1 1 1) samples are prepared in the same ultrahigh vacuum system on a clean nickel surface by a catalytic reaction of borazine $(BN)_3$-H_6 vapour according to recipes given in earlier publications [7,9]. In this way h-BN forms large terraces of a well-ordered monoatomic layer with a hexagonal 1×1 adsorbate structure (Figs. 1 and 2).

For the measurements, the sample atoms are excited by Si K_α X-rays ($h\nu = 1740.0$ eV). The intensity I of 884 eV photoelectrons from Ni $2p_{3/2}$ core levels ($E_B = 853$ eV) is then recorded at 5044 angular settings (θ, ϕ) which are uniformly distributed across the hemisphere above the sample surface (θ is the polar angle with respect to the surface normal and ϕ the azimuthal angle relative to some high symmetry crystal direction). Due to the high intensity of substrate emission measuring times of 1–2 s per setting are sufficient for yielding the high degree of statistical accuracy needed for this new difference method. The measurements are done for both h-BN/Ni and Ni samples using the same parameters.

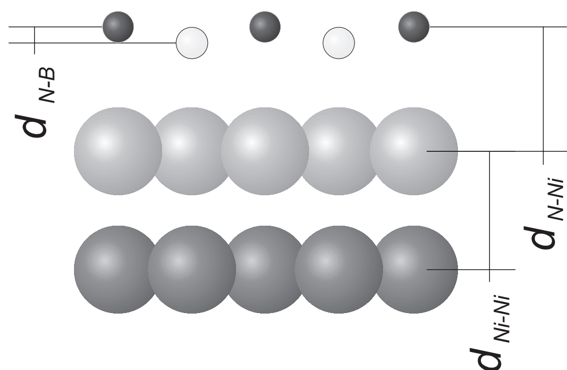

Fig. 2. Schematic layer structure of h-BN/Ni(1 1 1) (side view, same colours as in Fig. 1). Due to a very small lattice misfit h-BN forms a commensurate layer on Ni(1 1 1), but the B and N atoms are slightly out of plane [7]. The layer spacings found with XPD are $d_{N-B} = 0.07$ Å [7] and $d_{N-Ni} = 1.95$ Å (this study), the bulk Ni layer spacing is $d_{Ni-Ni} = 2.03$ Å.

3. Results and Discussion

The measured data sets are shown in Fig. 3. Obviously they show only minor differences that cannot be evaluated by eye. Furthermore, a theoretical calculation of the complex substrate pattern in such an accurate way that the h-BN effects could be interpreted directly is practically impossible due to computing power limitations. Fig. 4 shows the respective calculations for a three-layer approximation to the substrate; the calculation procedures will be explained later. Although the differences between the two diffraction patterns are bigger than in the measurements, the substrate influence still dominates the two pictures.

A remarkable improvement is achieved by subtracting the diffractograms $I(\theta, \phi)$ of the two samples (h-BN/Ni and Ni) according to

$$\Delta I(\theta, \phi) = \frac{1}{\alpha(\theta)} I_{\text{h-BN/Ni}}(\theta, \phi) - \frac{1}{\beta(\theta)} I_{\text{Ni}}(\theta, \phi). \quad (1)$$

For each of the θ-dependent normalization functions α and β a gaussian is fitted to the average values $\langle I \rangle(\theta)$ of azimuthal cuts in the θ-range from 0° to 70°. (Because of a rapid count rate drop towards grazing emission, which is an effect of our measuring geometry, we restrict the polar range to $\leqslant 70°$ for quantitative analysis. Nevertheless the pictures show the full data set.) The mathematical expression for the average values is given by

$$\langle I \rangle(\theta) = \frac{1}{N(\theta)} \sum_{\phi} I(\theta, \phi), \quad (2)$$

where $N(\theta)$ is the number of data points for the given θ. These values are also used in the so-called "ϕ-average" normalization which maximizes the azimuthal contrast and removes any ϕ-independent background from the diffractogram. Such a procedure is required for the h-BN/Ni case because the shape of the background is not reproduced in the simulations. Nevertheless a normal emission spot must be preserved in the normalization, which is accomplished by this "smooth ϕ-average" with the gaussian functions (this procedure is related to

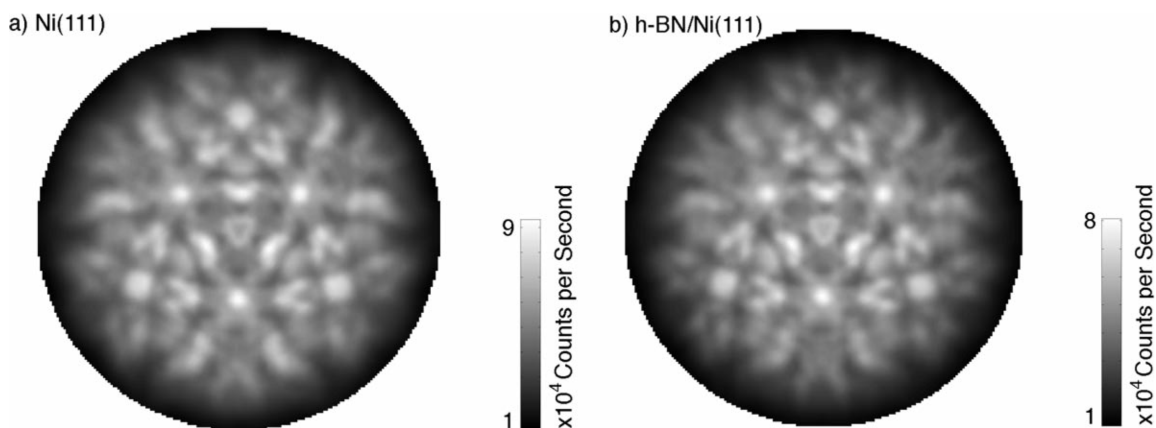

Fig. 3. Si K_α excited Ni 2p XPD patterns of a (a) Ni(1 1 1) and (b) h-BN/Ni(1 1 1) sample measured at room temperature. The 5044 angular settings are mapped stereographically where the top of the picture corresponds to the $[\bar{1}\,\bar{1}\,2]$ direction of the Ni crystal and the centre to [1 1 1] (normal emission). The edge of the picture corresponds to emission at a polar angle of 88°. The count rate is represented by a linear gray-scale.

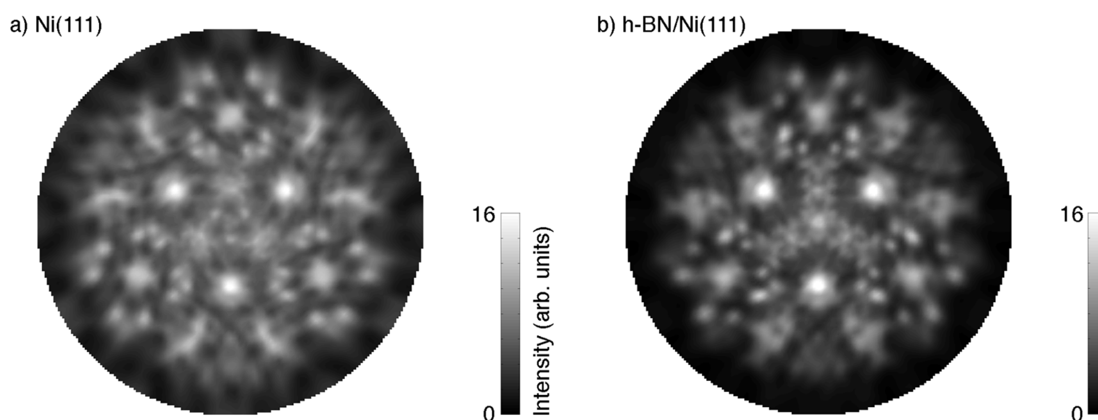

Fig. 4. Ni 2p XPD patterns of a (a) Ni(1 1 1) and (b) h-BN/Ni(1 1 1) sample with N-top geometry simulated by MSC.

the one introduced by Seelmann-Eggebert and Richter [10]).

The ΔI pattern of the measurements shown in Fig. 5a has been processed in such a way as outlined above. The remaining pattern differs completely from the substrate pattern (Fig. 3a) and therefore it must show mainly adsorbate effects. Its intensity variations correspond to an anisotropy of 19%, while the anisotropy

$$A = \frac{\max_{\theta \leqslant 70^\circ,\phi} I - \min_{\theta \leqslant 70^\circ,\phi} I}{\max_{\theta \leqslant 70^\circ,\phi} I} \qquad (3)$$

in the original diffractograms lies around 59%.

Fig. 5b addresses the question whether the difference pattern consists of spots from forward focusing at adsorbate atoms if one assumes the N-top geometry. Several bright features in the experimental data coincide with forward-scattering locations of electrons originating from the top nickel layer at nitrogen atoms whereas boron directions are under-represented or coincide with diffraction minima.

For a further interpretation of the data in Fig. 5a the procedure from Eq. (1) is repeated with

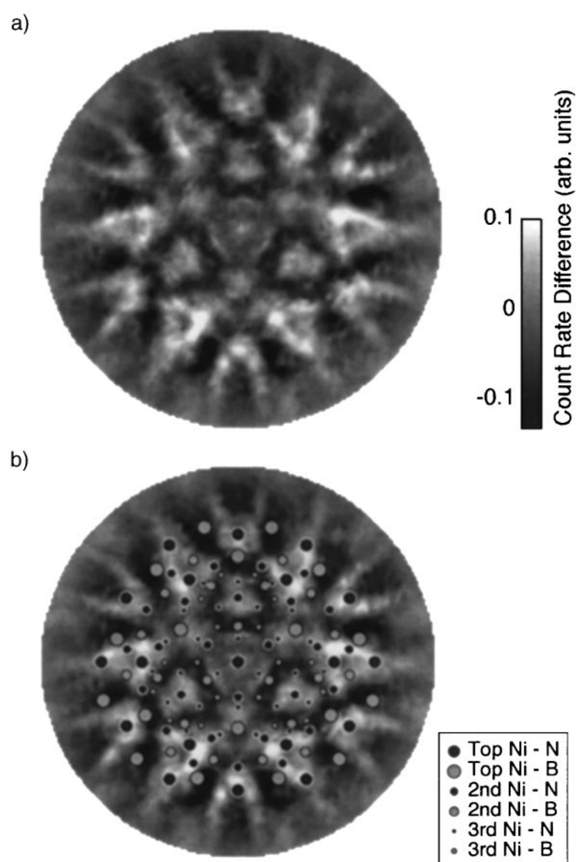

Fig. 5. (a) Difference pattern (adsorbate-covered sample minus clean substrate) from the measurements showing just the adsorbate effects. Assuming the N-top geometry (which is argued for in the text) subfigure (b) adds markers at directions where forward scattering at the adsorbate atoms is expected. Bright dots indicate scattering at boron and dark ones at nitrogen atoms. Their size refers to the emitting nickel layer.

simulated diffractograms for every possible geometry. These data sets are calculated according to multiple-scattering theory using a computer program developed by Kaduwela et al. [11]. (The benefit from multiple-scattering theory with respect to single-scattering will be pointed out later.) The calculations are based on an initial guess of the atomic structure of the sample, in our case derived from the well-known face-centered cubic nickel structure and the h-BN adsorbate structure known from earlier XPD measurements [7]. The structure model is then compiled into a "cluster" that describes the coordinates of the atoms in the neighbourhood of one designated photoemitting atom. For the Ni(1 1 1) sample the cluster was assembled of 37 Ni atoms distributed into three layers, 19 atoms in the top, 12 in the second and six in the third layer. In each layer one emitter atom near the layer centre is chosen and the results are averaged to threefold symmetry. For the h-BN/Ni cluster with N-top geometry, 19 nitrogen and 18 boron atoms are added, which gives a total of 74 atoms.

The cluster dimensions have been optimized with the subsequent diffractogram difference in mind. The most expressive features are expected at polar angles around 60° which correspond to scattering at the first and the second BN rings. This requires a sufficiently large diameter of the h-BN layer whereas the vertical extent of the substrate may be kept small.

The simulated diffractogram differences are shown in Fig. 6 for the three adsorbate geometries discussed above and parameter values mentioned in the caption of Fig. 2. Now, the experimental data in Fig. 5a can be visually compared to them. Neglecting the stronger angular broadening in the measurement and looking for corresponding high-intensity and low-intensity features at the same angles in the experimental and the simulated pictures, Fig. 6a (N-top geometry) reproduces them best, while the N-fcc simulation in Fig. 6c differs considerably from the experiment. Although in the N-hcp picture (Fig. 6b) some broad, threefold features catch the eye, their position and fine structure does not match the experimental picture. Of course, improvements to the simulation quality are desirable but would require larger clusters and thus much more computing time. [1]

The visual facts are also reflected in an R-factor analysis that compares the experimental and simulated difference data using the definition

[1] With the cluster size given in the text one h-BN/Ni simulation runs for about 4 h of CPU time on an Intel Pentium II-based computer.

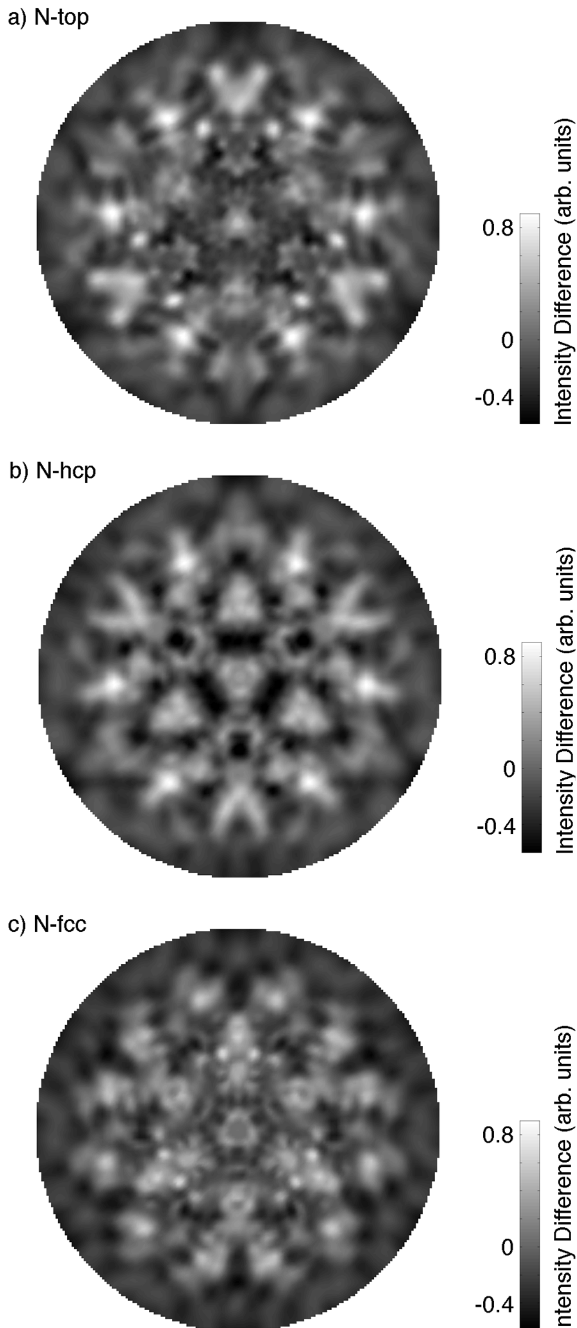

Fig. 6. Difference patterns (adsorbate-covered minus clean substrate) from MSC for the three structure models (a) N-top, (b) N-hcp and (c) N-fcc. They are compared to the experimental picture in Fig. 5.

$$R = \frac{\sum(\Delta I'_{\text{exp}} - \Delta I'_{\text{sim}})^2}{\sum(\Delta I'^2_{\text{exp}} + \Delta I'^2_{\text{sim}})}, \tag{4}$$

where the sums are over angles (θ, ϕ) with $\theta \leqslant 70°$. In order to equalize the anisotropies of experimental and simulated data sets the average values of the data sets are forced to 0 by subtracting a constant and the standard deviations to 1 by dividing by a constant (these scale-corrected data sets are labelled with primes). The normalization of R is chosen such that a value of 0 corresponds to perfect agreement, a value of 1 to uncorrelated data, and a value of 2 to anticorrelated data [12].

The R-factor values are listed in Table 1 for multiple-scattering (MSC) as well as single-scattering calculations (SSC). Both scattering levels clearly favour the N-top geometry while MSC gives some more confidence. The most important lack of the SSC diffractograms that we observe in our data sets is the well-known inaccuracy of SSC in estimating forward-focusing intensities along substrate atomic chains [11,13]. Since forward-focusing directions play an important role in our differential method the defocusing effect of multiple scattering along these chains has to be handled properly.

Fig. 7 shows the individual terms of the R-factor sum (4) in a diffractogram-like fashion. Here, bright colours report a big difference between experimental and simulated data. This is the case mainly for the N-fcc model. For N-top the differences are distributed evenly across the whole pattern but for N-hcp they concentrate around the meaningful 60° polar angle.

For a more detailed view on the anisotropies one can still extract azimuthal or polar cuts through decisive points from the diffractograms, as

Table 1
R-factors (from Eq. (4)) of the difference data compared to MSC and SSC calculations for the three structure models. Both simulation levels clearly favour the N-top registry. Compared to SSC, MSC improves mainly forward-scattering intensities along substrate atomic chains

	MSC	SSC
N-top	0.395	0.454
N-hcp	0.541	0.553
N-fcc	1.348	1.204

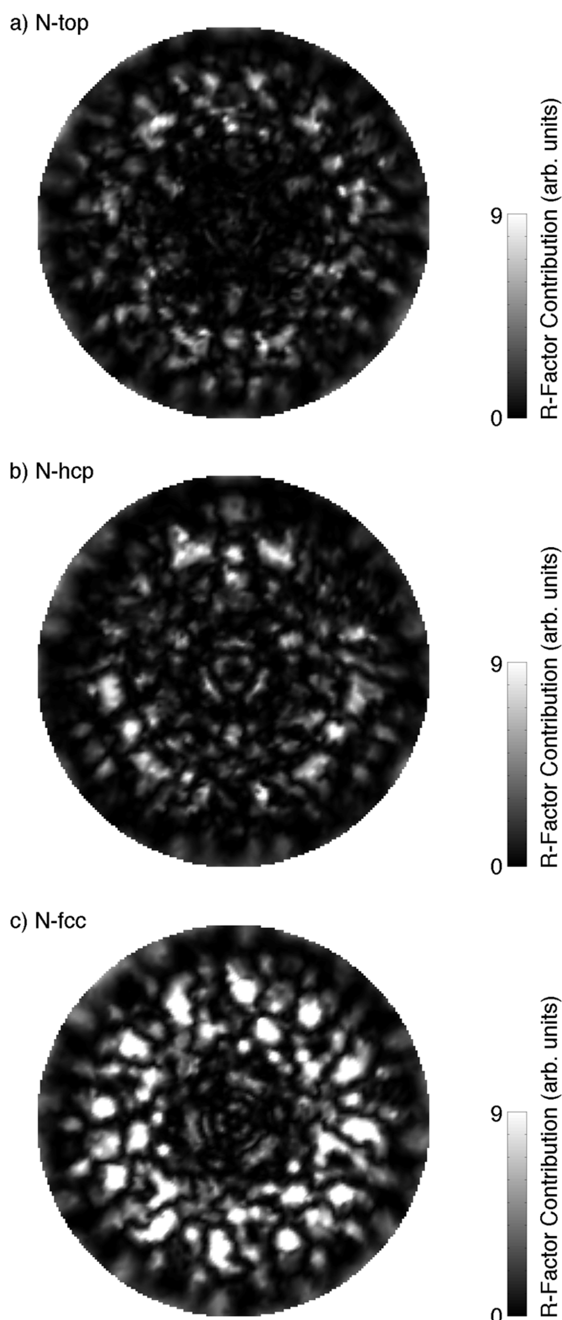

Fig. 7. Diffractogram-style R-factor maps show the squared differences of the experimental and each of the three h-BN/Ni models for an estimate of the matching quality in different angle regions. The gray-scale is chosen the same for all pictures while the calculated maximum values are 0.0012 (N-top), 0.0014 (N-hcp) and 0.0042 (N-fcc), respectively. The values are normalized as in Eq. (4).

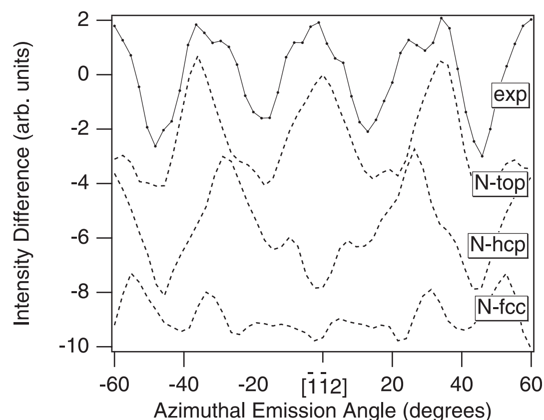

Fig. 8. Comparison of measured and simulated $\Delta I'(\phi)$ cuts at the polar angle $\theta = 60°$ in a two-dimensional plot. Only a 120° interval around $[\bar{1}\bar{1}2]$ is shown from the threefold symmetric picture. The experimental data have been averaged according to the same symmetry.

is shown in Fig. 8. Again, this graph clearly supports the N-top geometry.

It is also possible to extract structural parameters from the difference data if a series of simulations is carried out with systematically varied parameter values. As an example we refine the BN–Ni layer spacing $d_{\text{N–Ni}}$ in the N-top geometry while the corrugation $d_{\text{N–B}}$ is kept constant. The R-factors from Eq. (4) for different spacings in the N-top geometry are well approximated by a parabola the minimum of which indicates the best-fit value. The statistical error is estimated from $R_{\min} +$ var $R_{\min}$ and the corresponding $d_{\text{N–Ni}}$ interval. The variance of $R_{\min}$ is defined as

$$\text{var } R_{\min} = R_{\min}\sqrt{\frac{2}{N}}, \tag{5}$$

where N is the number of independent pieces of structural information contained in the experimental data [14], i.e. the number of inequivalent diffraction features that could be distinguished in the measured angle range. In our case, $N = \Delta\Omega/\delta\Omega \approx 230$, the ratio of the analysed and independent solid angle ($0° \leqslant \phi \leqslant 120°$, $0° \leqslant \theta \leqslant 70°$) and a 5° wide cone representing the smallest diffraction spot size observed in the measurements. We obtain $d_{\text{N–Ni,XPD}} = (1.95 \pm 0.16)$ Å. This value

lies somewhat below $d_{\mathrm{N-Ni,LEED}} = (2.22 \pm 0.07)$ Å found from LEED [6].

4. Conclusions

A difference method for the analysis of adsorbate structures based on angle-scanned photoelectron diffraction has been introduced. It takes advantage of the element sensitivity of XPD, which permits to obtain different perspectives on the atomic neighbourhood, and specifically looks at the adsorbate from the perspective of the topmost substrate layers. The visualization feature of angle-scanned XPD allows an intuitive and unambiguous characterization of the atomic structure when combined with simulation techniques and the interpretation of forward-scattering directions. The difference method is especially suitable for determining the adsorbate–substrate registry in interface structures.

Its practical use for a compact and homogeneous layer has been demonstrated on the h-BN/Ni(1 1 1) system where the registry can be clearly discriminated, although the precision of extracted parameter values is limited by the instrumental angular resolution and the intrinsic angular width of diffraction features. Due to the high intensity of substrate photoemission short measuring times are achieved, and, because one is always in the forward-scattering regime, sample cooling is not required. On the theoretical side, the atomic clusters can be held sufficiently small to allow quick MSC on modern workstation computers.

We expect that this method can be successfully applied to a wide variety of similar adsorbate systems. Besides the limitations of conventional angle-resolved photoelectron diffraction (like macroscopic domain averaging or the need for sufficiently high scattering factors and scatterer densities) the one important prerequisite for this new method to work is that the substrate surface is not significantly reconstructed in the clean or the adsorbate-covered state. Of course, the substrate structure has to be known before, and a preceding investigation of the adsorbate structure considerably facilitates the refinement of the structure model.

Acknowledgements

We are grateful to Prof. Heinrich Nöth for the production of borazine and to Werner Deichmann for the technical support. This work has been supported by the Swiss National Science Foundation.

References

[1] J. Osterwalder, P. Aebi, R. Fasel, D. Naumović, P. Schwaller, T. Kreutz, L. Schlapbach, T. Abukawa, S. Kono, Surf. Sci. 331–333 (1995) 1002.
[2] J. Wider, T. Greber, E. Wetli, T.J. Kreutz, P. Schwaller, J. Osterwalder, Surf. Sci. 417 (1998) 301.
[3] T. Greber, J. Wider, E. Wetli, J. Osterwalder, Phys. Rev. Lett. 81 (1998) 1654.
[4] E.D. Tober, R.X. Ynzunza, F.J. Palomares, Z. Wang, Z. Hussain, M.A. Van Hove, C.S. Fadley, Phys. Rev. Lett. 79 (1997) 2085.
[5] C.S. Fadley, M.A. Van Hove, Z. Hussain, A.P. Kaduwela, R.E. Couch, Y.J. Kim, P.M. Len, J. Palomares, S. Ryce, S. Ruebush, E.D. Tober, Z. Wang, R.X. Ynzunza, H. Daimon, H. Galloway, M.B. Salmeron, W. Schattke, Surf. Rev. Lett. 4 (1997) 421.
[6] Y. Gamou, M. Terai, A. Nagashima, C. Oshima, Sci. Rep. RITU A 44 (1997) 211.
[7] W. Auwärter, T.J. Kreutz, T. Greber, J. Osterwalder, Surf. Sci. 429 (1999) 229.
[8] T. Greber, O. Raetzo, T.J. Kreutz, P. Schwaller, W. Deichmann, E. Wetli, J. Osterwalder, Rev. Sci. Instrum. 68 (1997) 4549.
[9] A. Nagashima, N. Tejima, Y. Gamou, T. Kawai, C. Oshima, Phys. Rev. B 51 (1995) 4606.
[10] M. Seelmann-Eggebert, H.J. Richter, Phys. Rev. B 43 (1991) 9578.
[11] A.P. Kaduwela, D.J. Friedman, C.S. Fadley, J. Electron. Spectrosc. Relat. Phenom. 57 (1991) 223.
[12] P. Hofmann, K.-M. Schindler, S. Bao, V. Fritzsche, A.M. Bradshaw, D.P. Woodruff, Surf. Sci. 337 (1995) 169.
[13] S.Y. Tong, H.C. Poon, D.R. Snider, Phys. Rev. B 32 (1985) 2096.
[14] N.A. Booth, R. Davis, R. Toomes, D.P. Woodruff, C. Hirschmugl, K.-M. Schindler, O. Schaff, V. Fernandez, A. Theobald, P. Hofmann, R. Lindsay, T. Gießel, P. Baumgärtel, A.M. Bradshaw, Surf. Sci. 387 (1997) 152.